

TIME RESOLVED PARTICLE IMAGING VELOCIMETRY FOR THE INVESTIGATION OF ROTATING STALL IN A RADIAL PUMP

by

N. Krause, K. Zähringer, E. Pap
Otto-von-Guericke Universität Magdeburg
Universitätsplatz 2
39116 Magdeburg Germany

ABSTRACT

In industrial applications, turbomachineries are not only used in their design point, but also at significant lower or higher flow rates. This operating range is limited on the low flow rate side by instabilities in flow leading parts of the machinery. In these operating points, vortices are created, which are caused by the detachment of the boundary layer from the walls of the flow leading parts of the machine, e. g. in the impeller. These one or more stall cells can start to propagate in the impeller at a fraction of the rotor speed, if the flow is throttled further.

In this study we investigate by time resolved PIV the different stages of rotating stall in a radial pump. This technique allows us to investigate the flow field in every channel of the impeller. Thus measurements in transient and unsteady flows of rotating turbomachinery become possible with these systems. In our study, we used a frequency of 50 Hz and a CMOS-camera with 1280x1024 pixel, to record a flow field of 143.52x114.816 mm². This results in one velocity vector every 1.794 mm. This set-up allowed the acquisition of 510 double pictures at a frequency of 50 Hz. With an impeller consisting of 5 blades and a rotational speed of 600 r.p.m.. This means that in each channel the flow fields could be measured during 102 rotations of the impeller.

The results will presented here have been obtained at different operating points. It was possible to observe different stages of the developing rotating stall. The first vortices were observed at a throttled flow rate of 50% of the design point. They existed only in one channel of the impeller. The first rotations of the stall cell through the impeller could be observed at flow rates smaller than 40% of the design point. These velocity fields allowed further conclusions about the possible development of the rotating stall cell. An example is presented in figure 1 where the whole channel is blocked.

In order to calculate the angular speed of the rotating stall in the impeller, we applied frequency analysis to the measured flow fields. FFT-analysis was applied to the 510 vector fields of one measurement series, for each velocity vector separately and for both, its direction and magnitude. To get a characteristic frequency spectrum of the whole flow field, the normalised sum of the separate frequency spectra of each vector was calculated. Figure 2 presents an example of the result of the frequency analysis. The results show that the velocity vectors change with a different frequency as the impellers rotational speed. The changing frequency of the flow field and thus the rotating stall speed have been determined in that way from the measured velocity fields.

This study demonstrates the importance of time resolved PIV in the understanding of the rotating stall phenomenon, as it allows to measure and visualise transient, irregularly appearing flow fields.

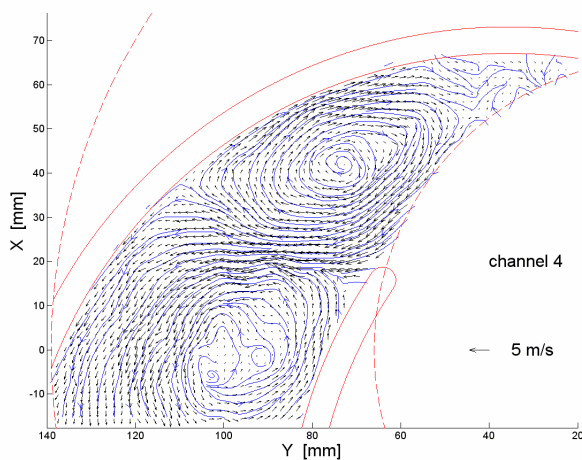


Fig. 1 Relative velocity with streamlines in a blocked channel at $Q/Q_0=0.35$

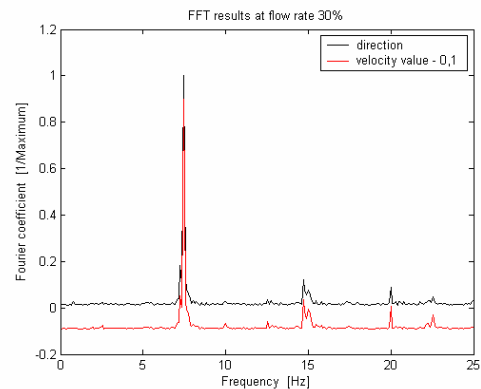


Fig. 2 FFT results at $Q/Q_0=0.3$

1 INTRODUCTION

The different velocity components of the flow through a rotating impeller are presented graphically by velocity vectors (figure 3). The shape of such vector diagrams in consideration of the peripheral velocity u of the impeller is triangular and they are called velocity triangles. The relative velocity w of flow is considered relative to the impeller. The absolute velocity of flow is taken with respect to the pump casing and is always equal to the vectorial sum of the relative velocity w and the peripheral velocity u of the impeller, $c = w + u$. Any point on the impeller will describe a circle around the shaft axis and will have a peripheral velocity $u = r \times \omega$ where r is the radius of the circle and ω is the angular velocity of the impeller. Figure 3 presents the flow around an impeller blade at inlet part at the design point where the flow is optimum and the stagnation point is on the blade cusp.

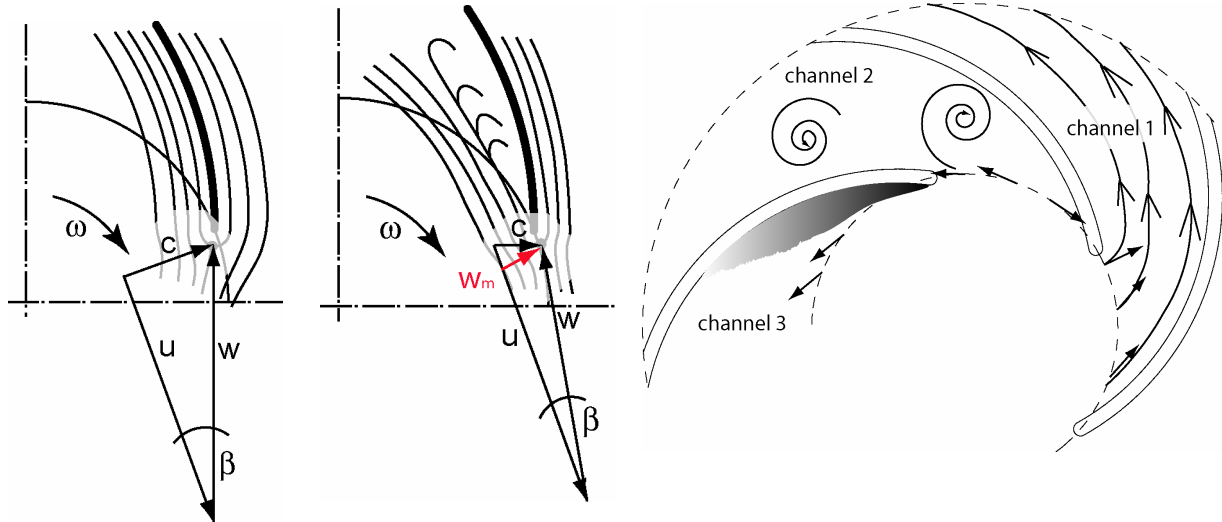


Fig. 3 Flow around an impeller blade at design point. *Fig. 4 Flow around an impeller blade at partial capacity.* *Fig. 5 Rotating Stall phenomenon in a radial impeller.*

When the flow rate is reduced, the meridional component of the relative velocity w_m also decreases. With these reduced flow rates the angle of attack rises and the stagnation point is displaced to the pressure side of the blade. When the angle of attack is oversized the flow on the suction side will be detached and stall can appear (figure 4). The static pressure inside the stall region is smaller than in the surrounding flow, therefore vortices can form with the same rotating direction as the impeller. In the outlet of the channel a second vortex can be formed with an inverse rotational direction (exchange vortex, channel 2 in figure 5). These vortices can increase in size until the complete channel is blocked. Then, the medium has to pass through the following channel (channel 3 in figure 5). This leads once more to a displacement of the stagnation point, this time in channel 3, and a new stall cell will be formed in this channel. On the other hand, the flow in channel 1 will reattach and the flow conditions in this channel will be good once more. It is possible that not only one stall cell exists in the impeller but also more. With this mechanism, the stall cells can turn around through the impeller. Because the angular velocity of the stall cell is lower than the impeller angular velocity, the stall cell turns inside the impeller against the rotational direction of the impeller. This description of the rotating stall phenomenon was first published by Emmons et al., 1955.

The main problem for the investigation of flow instabilities is the unsteadiness of the whole flow field. With Laser-Doppler-Velocimetry (LDV) measurements high acquisition frequencies are attained, but only a point-by-point analysis can be done. With standard PIV systems, the flow field can be investigated as a whole, but the time resolution is very poor, thus preventing a correct analysis of the unsteady character of the flow. Sieverding (Sieverding et al., 2000) gives an overview of measurement techniques for unsteady flows in turbomachineries, which includes pressure sensors, temperature sensors and hot wire measurement systems. These techniques also allow only point-by-point acquisitions, but not the analysis of the complete flow field at the same time. Previous measurements of the rotating stall phenomenon used these kind of measurement systems, most of which are intrusive techniques. Investigations with hot-wire probes (Day, 1993, Garnier et al., 1991, Place et al., 1996) and pressure probes (Dobat et al., 2001, Escuret & Garnier, 1996, Garnier et al., 1991, Höss et al., 2000, Inoue, 2000, Saxer-Felici et al., 1999, Surek, 2001, Ulbricht, 2002) could verify the periodicity of the rotating stall cell. In this case it was not possible to investigate the complete flow field of the stall cell. A further problem of previous measurements is that phase averaging was applied. This means that the stochastic character of the phenomenon and significant attributes which are not exactly periodic are lost. In previous

investigations it was not clear, how the structure of the stall cell is composed (Katz, 2002). Wernet (Wernet, 2000) used pressure probes in order to trigger a standard PIV system at the onset of unsteady flow phenomena in a centrifugal impeller. This technique, based on two different measurement systems, allowed the visualisation of the reverse flow in the impeller passage. A systematic investigation of the reverse flow was not possible by this technique and the author claims that the “lack of conclusive evidence of the flow reversing through the impeller may only be the result of not capturing the surge flow at the right instant in time”.

This shows, that the investigation of such flows should not use averaged or point wise methods, but has to be performed with a high temporal and spatial resolution. New technologies in laser and camera technique now give the possibility to deepen previous knowledge and clarify the structure of the stall cell.

In this study we present such time-resolved PIV-measurements of the whole flow field in a centrifugal pump, which is subject to rotating stall, when working in partial capacity regimes. These measurements show the capability of the measuring system of capturing the stall phenomenon and allow its systematic investigation. A frequency analysis of the obtained flow fields allowed the determination of the stall rotating frequency inside the impeller.

2 EXPERIMENTAL SET-UP

The experimental set-up used for this study is presented in figure 6. The water circuit and transparent radial pump have been used in other investigations before and are presented in detail in Pap & Lanzke, 1999 and Pap et al., 2001.

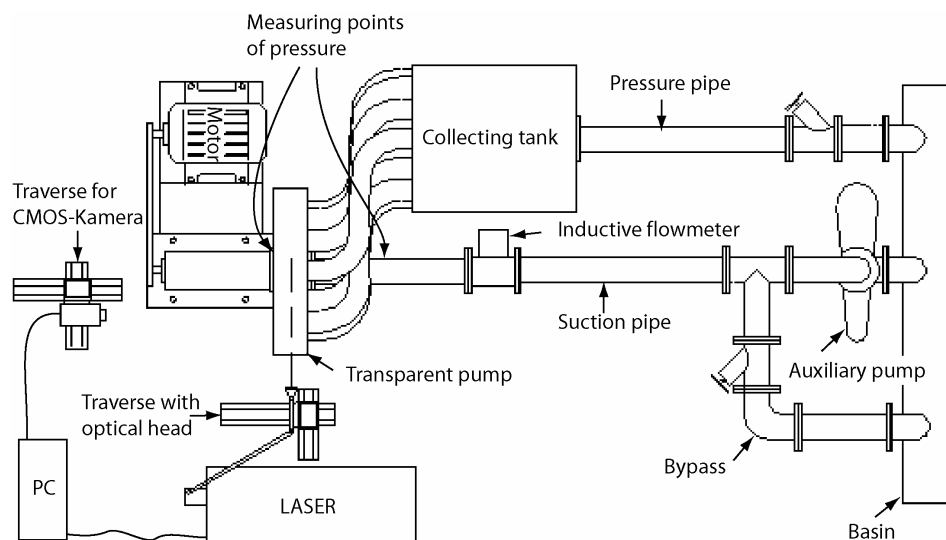


Fig. 6 Scheme of the radial transparent pump installation with PIV measurement system

The investigated transparent radial pump is situated in a water circuit, which is fed by an auxiliary pump with a bypass for a constant static pressure in the suction pipe before the investigated pump. The inductive flow meter measures the volume flow, which can be adjusted by a hand valve in the pressure pipe. Pressure probes in the suction pipe and after the impeller measure the static pressure before the pump and the pressure difference over the impeller. With these components it is possible to get reproducible operating points.

2.1 „TIME RESOLVED“ PIV MEASURING SYSTEM

The frequency doubled Nd:YAG-Laser used for the experiments has a variable repetition rate from 10 Hz to 5 kHz and allows pulse intervals from 1 μ s to 100ms, with a pulse duration of 75 ns and an energy of 2 x 12.5 mJ at a repetition rate of 50 Hz. The time between two laser pulses used for the experiments presented here was 120 μ s. The thickness of the light sheet inside the pump is approximately 1 mm. The light sheet is adjusted in a way that it is vertical to the shaft axis in the centre of the channel width. The open angle of the light sheet optics is 14°, in this case it is possible to measure a section of one of the blade channels.

The resolution of the high speed PIV camera is variable and is reduced at higher repetition rates. The resolution used here was 1280x1024 Pixels at 50 double images per second. The memory size of the CMOS-camera was 4 GB, so that 510 double images could be recorded at once. Because the impeller of the pump has 5 blade channels we thus could record 102 revolutions of the impeller, which means a record duration of 10.2 s. The PIV-camera was mounted on a traversing system, perpendicular to the light sheet plane of the laser. A Nikon f=50mm, f/2.4 objective was used with a 590nm high pass filter in front of it. With these optical settings the investigated area in

the impeller of the pump had a size of 143.52x114.816 mm². This results in one velocity vector every 1.794 mm, when using an interrogation area of 32 x 32 pixel with 50 % overlap.

To reduce reflections of the laser light from parts of the impeller Rhodamin B doped melamine resin tracer particles have been used. Rhodamin B is stimulated to fluorescence by the Nd:YAG-Laser and emits light with a wave length from 550 to 610 nm. To separate the fluorescence light from the laser light we used a high pass filter with a cut off wave length of 590 nm in front of the PIV-camera. The mean particle size was 5.3 μm, with 90% of the particles having a size smaller than 9.7 μm.

2.2 CENTRIFUGAL PUMP

Parts of the pump case and the impeller are made of acrylic glass to get good optical access (figure 7). The drawback is the less mechanical strength of acrylic in comparison to metallic materials. The pump is constructed in a way, that a rotationally symmetric pressure distribution can be obtained. Therefore the impeller is followed by a circular diffusor with 12 drain pipes.

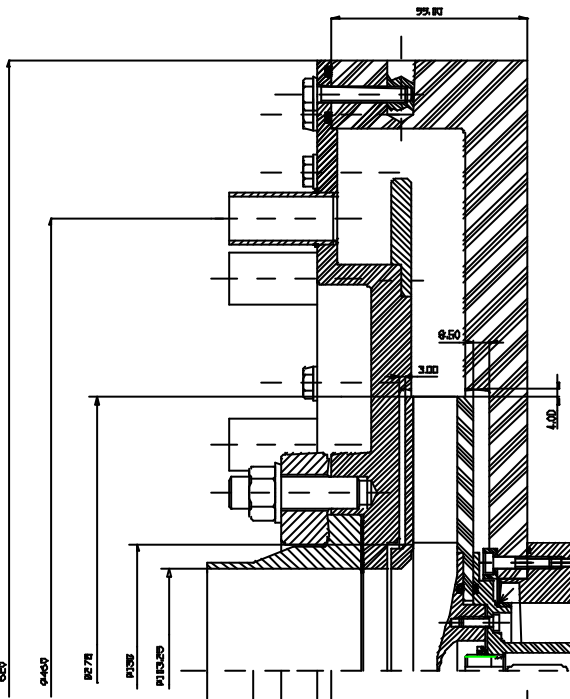


Fig. 7 Geometry of the pump (meridian section)

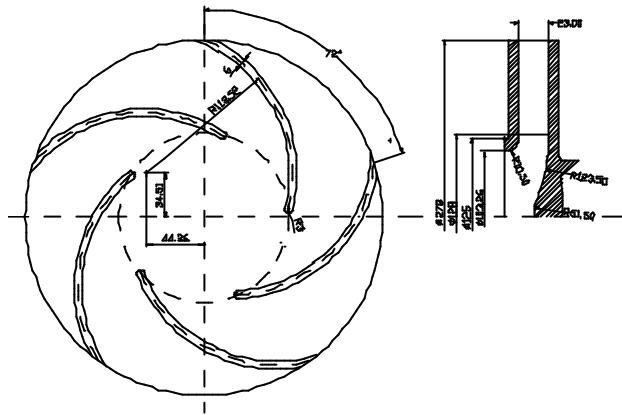


Fig. 8 Geometry of the impeller

The blades of the impeller are constructed as arcs of a circle. Both the blades and the back shroud are of acrylic. The blade angle at the inlet of the blade channel is 19° and at the outlet 23°. Figure 8 shows the geometry of the impeller. The geometrical attributes guarantee an inflow without shock at the nominal flow rate Q_0 of 47,5 m³/h. For the drive of the pump a synchronous motor is used, it drives the pump with a toothed belt in a gear transmission ratio of 1:1. A synchronous motor is used because it follows the power frequency slip free. Therefore the number of revolutions of the pump can be regulated by a frequency transformer. The number of revolutions used in these experiments was 600 r.p.m..

2.3 PUMP CHARACTERISTIC

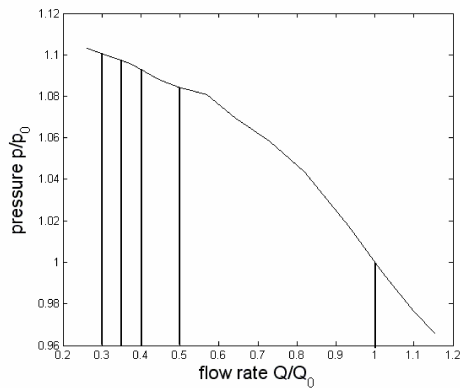


Fig. 9 Pump characteristic with the flow rates used in the measurements

Figure 9 shows the pump characteristics determined for the transparent radial pump. The pressure p and the flow rate Q are related to the nominal pressure p_0 and flow rate Q_0 of the machine. The line shows the pump characteristic for decreasing flow rate. Stall cells could be seen first at a flow rate of $Q/Q_0=0.5$. The vertical lines in figure 9 represent the different regimes used for this study at nominal flow rate ($Q/Q_0=1$) and at throttled flow rates of 50, 41, 35 and 30 % of the nominal flow.

3 RESULTS

Figure 10 shows the region of the impeller imaged by the camera with a red quadrangle. Every pump channel is imaged in the same position since the rotational speed of the pump (600 rpm) and the double image frequency (50 Hz) of the camera are adjusted in that way. The channels have been numbered in the following in the way represented in figure 10. In the following the images are presented twisted 90° to the left for image formatting reasons.

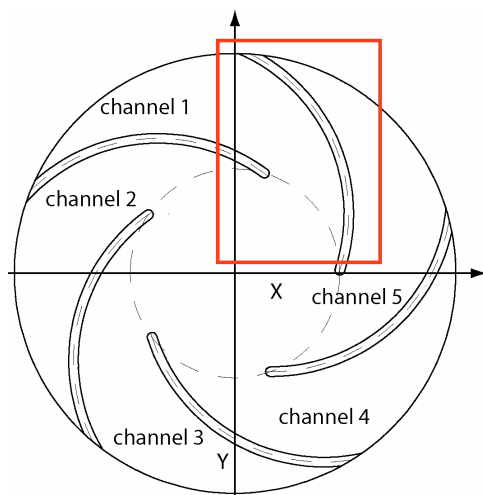


Fig. 10 Measured flow field in the impeller and numbered channels

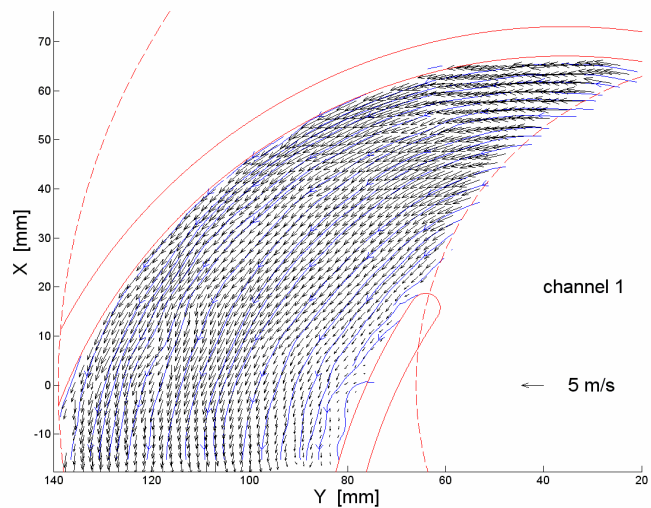


Fig. 11 Flow field in channel 1 at $Q/Q_0=1$

3.1 DESIGN POINT

In figure 11 the flow field at nominal flow rate ($Q/Q_0=1$) in channel 1 of the impeller is presented. In this channel only small stochastic disturbances are identifiable. As expected, the flow field shows higher velocities at the suction side and smaller velocities on the pressure side of the blades. The stream lines (blue lines) follow the blade contour. The flow is optimum.

3.2 PARTIAL CAPACITY WITHOUT ROTATING STALL

In the case of a flow rate of $Q/Q_0=0.5$ a standing stall cell could be observed in one channel of the impeller. Over the record duration of 10.2 s the stall cell stays in channel 2, which is presented in figure 13. The pictures of one revolution of the impeller, which are presented here (figure 12 to figure 16), are representative for all 102 revolutions. In channel 1 (figure 12) and channel 3 (figure 14) the flow is more disturbed than in channel 4 (figure 15) and channel 5 (figure 16), which are not in the neighbourhood of the disturbed channel 2. The flow perturbation in channel 3 is not stochastic, because the disturbances at coordinates around $x=10\text{mm}$ and $y=90\text{mm}$ are visible in all other pictures of channel 3. These pictures show that before rotating stall establishes, stall cells exist in particular channels of the impeller. The vortices of the stall cell here do not completely block the blade channel. The flow can pass on the pressure side of the channel.

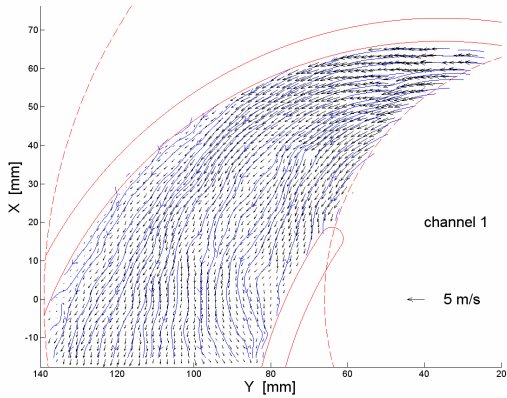


Fig. 12 Flow field in channel 1 at $Q/Q_0=0.5$

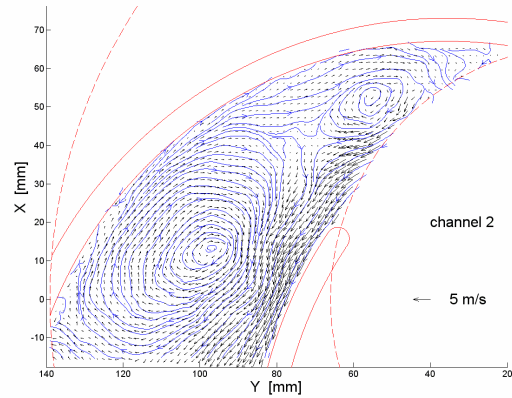


Fig. 13 Flow field in channel 2 at $Q/Q_0=0.5$

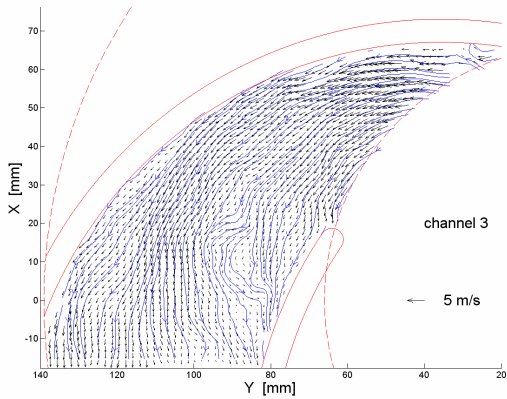


Fig. 14 Flow field in channel 3 at $Q/Q_0=0.5$

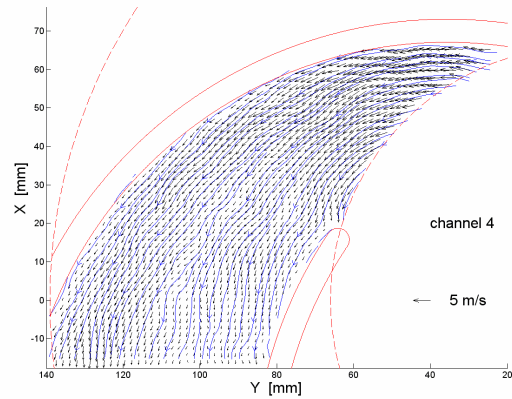


Fig. 15 Flow field in channel 4 at $Q/Q_0=0.5$

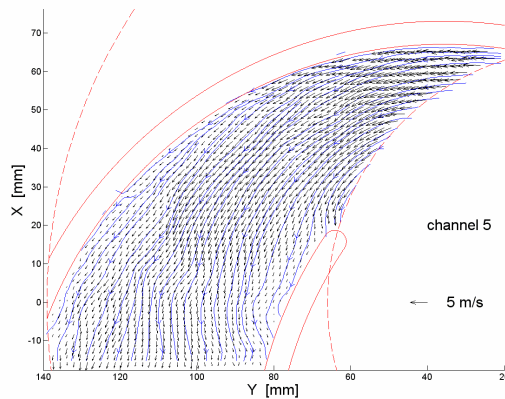


Fig. 16 Flow field in channel 5 at $Q/Q_0=0.5$

3.3 PARTIAL CAPACITY WITH ROTATING STALL

At a flow rate of $Q/Q_0=0.41$ the stall cells could not only be observed in one, but in several channels of the impeller. In this operating point the stall cell moves through the impeller with an angular velocity different from that of the impeller. The stall cell appears turning in the inverse sense of the impeller movement. Table 1 summarises the existence of stall cells in the different blade channels, during 102 revolutions of the impeller. Channels in which a vortex could be observed are denoted by **X**, channels without a vortex are denoted by 0.

Table 1 Table of the observed vortices in the channels of the impeller at $Q/Q_0=0.41$

revolution	channel 1	channel 2	channel 3	channel 4	channel 5	revolution	channel 1	channel 2	channel 3	channel 4	channel 5	revolution	channel 1	channel 2	channel 3	channel 4	channel 5	revolution	channel 1	channel 2	channel 3	channel 4	channel 5
1	0	X	X	0	0	21	0	X	X	0	X	35	0	X	X	0	0	82	0	0	0	0	X
...	0	X	X	0	0	22	0	0	0	0	X	...	0	X	X	0	0	83	0	X	0	0	0
9	0	X	X	0	0	23	X	X	0	0	0	52	0	X	X	0	0	84	0	X	X	0	0
10	0	0	0	X	X	24	X	X	0	0	0	53	0	0	X	X	X	...	0	X	X	0	0
11	X	0	0	0	X	25	0	X	0	0	0	54	0	0	0	X	X	89	0	X	X	0	0
12	X	0	0	0	0	26	0	X	X	X	0	55	0	0	0	0	X	90	0	0	X	X	0
13	X	0	0	0	0	27	0	0	X	X	X	56	0	X	0	0	X	91	0	0	0	X	X
14	X	X	0	0	0	28	0	0	0	X	X	57	0	X	0	0	0	92	X	0	0	0	X
15	X	X	0	0	0	29	0	0	0	X	X	58	0	X	X	0	0	93	X	X	0	0	0
16	X	X	0	0	X	30	0	0	0	0	X	...	0	X	X	0	0	94	0	X	0	0	0
17	X	X	0	0	0	31	0	0	0	0	X	78	0	X	X	0	0	95	0	X	X	0	0
18	0	X	0	0	0	32	0	0	0	0	X	79	0	0	X	0	0	...	0	X	X	0	0
19	0	X	X	0	0	33	0	0	0	0	X	80	0	0	X	X	X	102	0	X	X	0	0
20	0	X	X	0	X	34	0	X	0	0	0	81	0	0	0	X	X						

It can be recognised that the stall cells stay for several revolutions of the impeller in two specific channels. More often than not they are stabilised in blade channels 2 and 3. Channel 2 is the same channel in which a first stall cell has been observed at the higher flow rate of $Q/Q_0=0.5$, but without moving through the impeller. The localisation in a specific channel leads to the conclusion that in spite of the computer-aided manufacturing of the parts of the pump, there must exist irregularities in the geometry of the pump. These irregularities are very small, but apparently sufficient to induce small unsymmetrical flow distributions to the channels, which, then are at the origin of the rotating stall cell.

Figure 17 to figure 25 present a selected successive image series for a flow rate of $Q/Q_0=0.35$. The series is haphazardly chosen from the 510 images of one experiment series. It is characteristic for the 510 images of the whole series. The nomenclature of the channels follows the pattern (number of the channel)_(impeller revolution in relation to the first presented image). At this flow rate the stall cell turns through the impeller. It can be observed that a particular flow pattern repeats every 6 or 7 images, independently from the actual blade channel number.

In figure 17 and figure 18 nearly ideal flow fields, after the passing of a stall cell can be observed. The same flow pattern is visible in figure 24 and figure 25.

In figure 19 and figure 20 the flow field of channels 3 and 4 is represented during the first revolution of the impeller. In channel 3_1 a distinct, rather big and a small vortex core are identifiable. These vortices have the same spin. In contrast to this, in channel 4_1 the two very big vortex cores are spinning in opposite directions. The vortex on the suction side of the blade, on the entry of the channel is turning clockwise, the vortex located on the pressure side of the blade is spinning counter clockwise. In channel 4_1 the flow is nearly completely blocked, it is dominated by the two stall cells..

In channel 5_1 (figure 21) and channel 1_2 (figure 22) a stall cell is born, whereby the vortex in channel 5_1 is already in a later state than in channel 1_2. The flow velocity between the vortex and the pressure side of the channel is increased. In channel 1_2 the first phase of the stall cell is visible. The flow detaches at the entrance of the channel on the suction side of the blade and a reverse flow zone establishes.

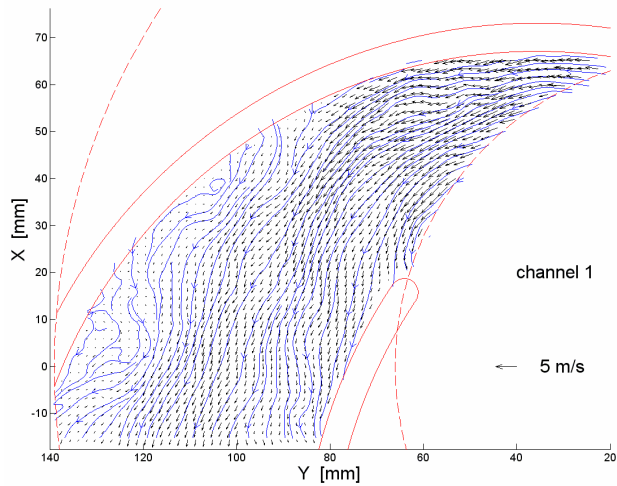


Fig. 17 Flow field in channel 1_1 at $Q/Q_0=0.35$

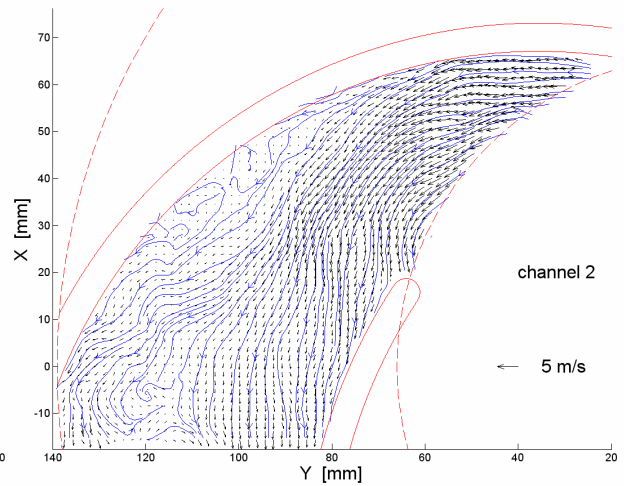


Fig. 18 Flow field in channel 2_1 at $Q/Q_0=0.35$

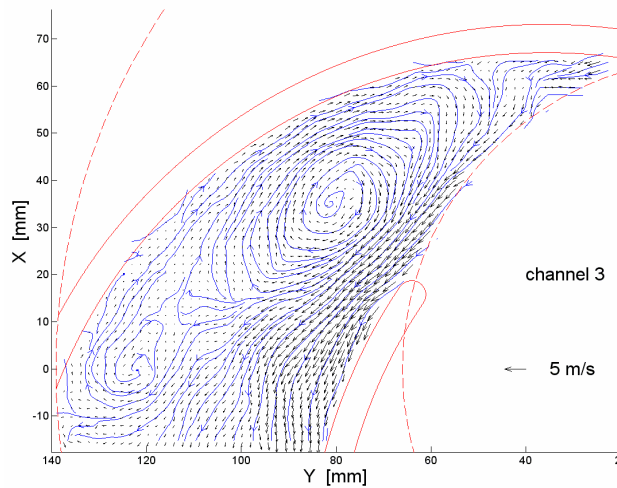


Fig. 19 Flow field in channel 3_1 at $Q/Q_0=0.35$

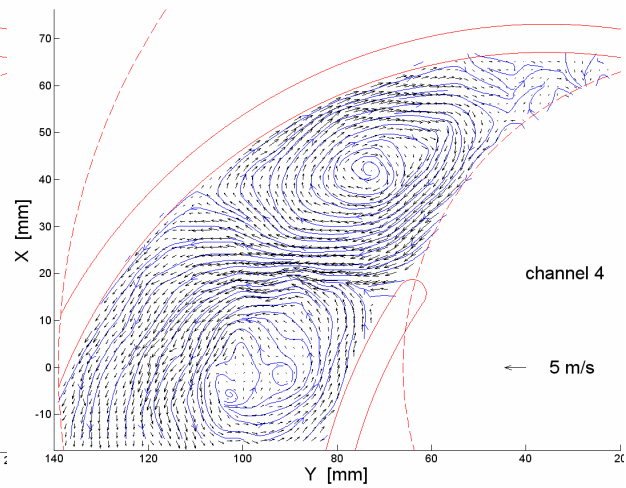


Fig. 20 Flow field in channel 4_1 at $Q/Q_0=0.35$

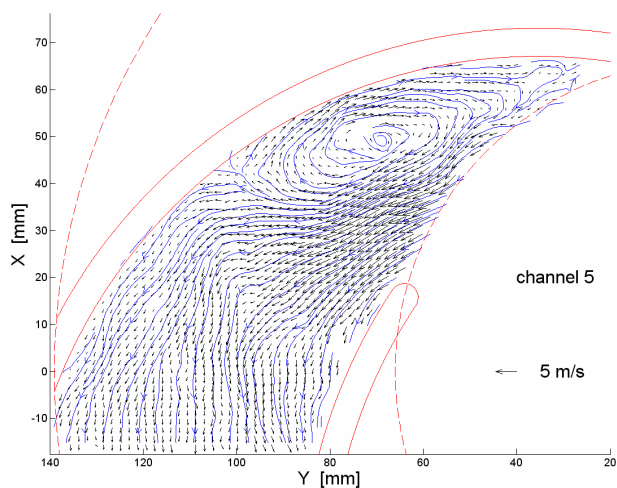


Fig. 21 Flow field in channel 5_1 at $Q/Q_0=0.35$

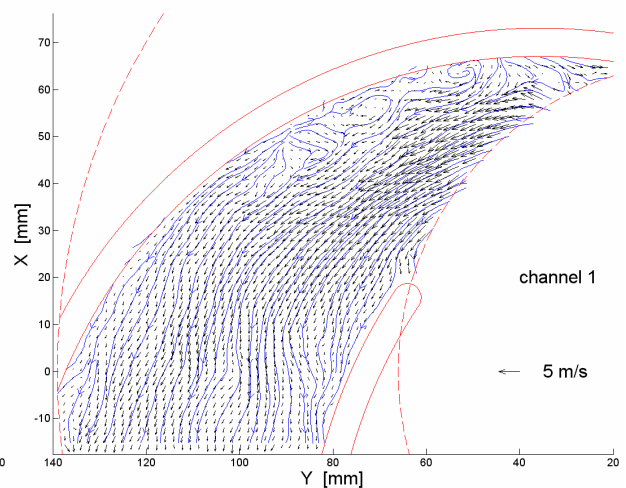


Fig. 22 Flow field in channel 1_2 at $Q/Q_0=0.35$

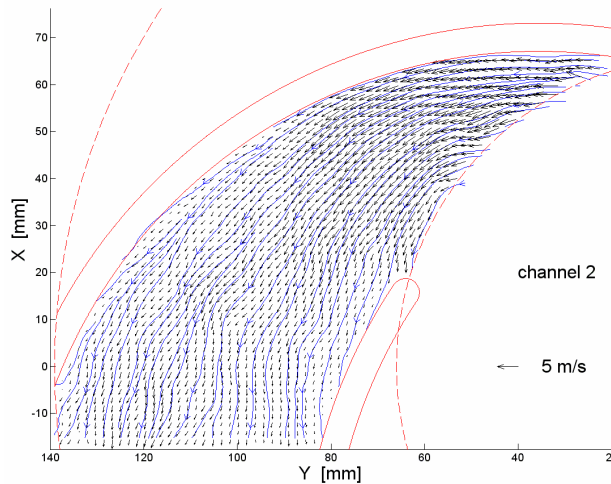


Fig. 23 Flow field in channel 2_2 at $Q/Q_0=0.35$

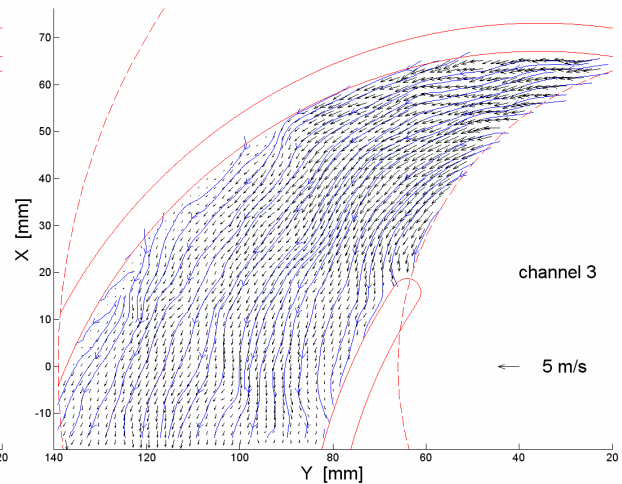


Fig. 24 Flow field in channel 3_2 at $Q/Q_0=0.35$

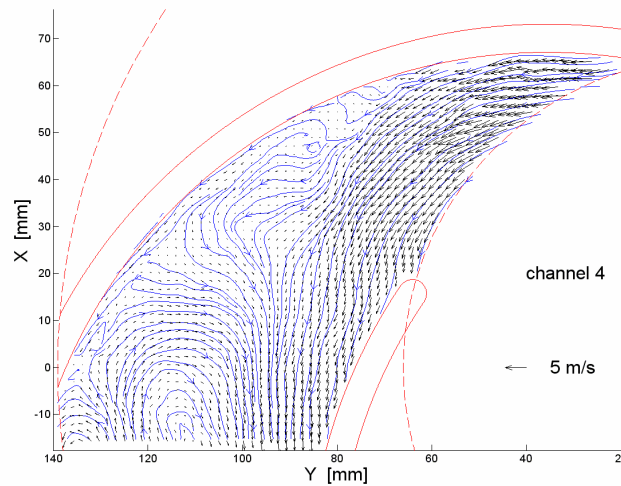


Fig. 25 Flow field in channel 4_2 at $Q/Q_0=0.35$

To prove that the stall cell is visible in a similar stadium after 6 or 7 images, channel 4_2 is presented in figure 25. Its flow pattern corresponds to that in figure 19 or 20. A big vortex can be seen once more, which has established at the outlet of the channel near the suction side of the blade. In the entry of the channel the flow field becomes regular.

The repeatability of the flow pattern every 6 or 7 images could be recognised on all experimental series done for the mentioned flow conditions. In order to verify this observation mathematically, the measured velocity fields have been frequency analysed by FFT calculations.

4 FREQUENCY ANALYSIS

In chapter 3.3 before the changing structures of the flow field in the single channels of the impeller at different flow rates could be observed. The velocity vectors composing these characteristic structures can be analysed in terms of frequencies, since the time lag between two successive vector fields is known, from the experimental conditions (here $\Delta t=20\text{ms}$). For this analysis the fast-fourier-transformation (FFT) was used within a Matlab R13 (TheMathWorks, 2002) algorithm.

Figure 26 presents the measured magnitude of the velocity for a single point in the flow field in function of the time. Figure 27 presents the time series for the velocity direction in the same point. The selected point has the coordinates $x=25.7\text{ mm}$ and $y=105.1\text{ mm}$ at a flow rate of $Q/Q_0=0.35$. This means that this point is situated near the suction side of the impeller channels.

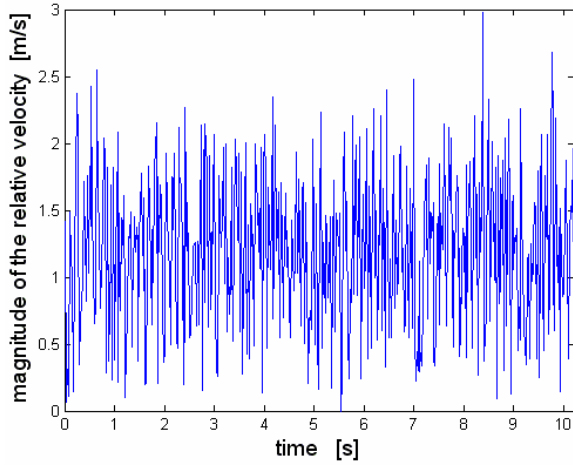


Fig. 26 Magnitude of the relative velocity in function of the time

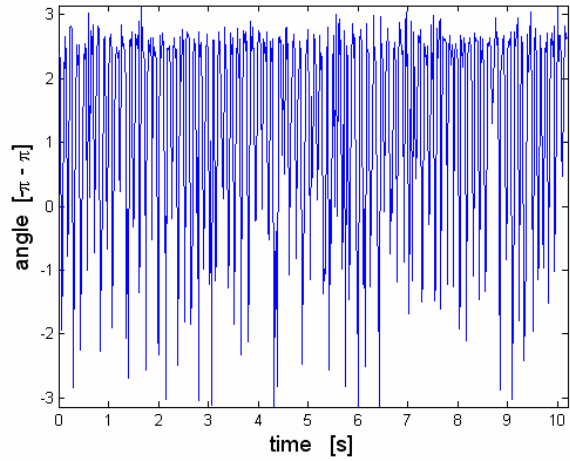


Fig. 27 Direction of the relative velocity in function of the time

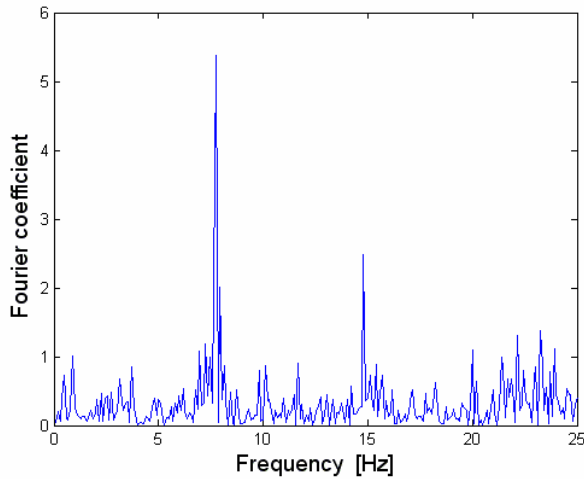


Fig. 28 FFT-spectrum of the relative velocity magnitude

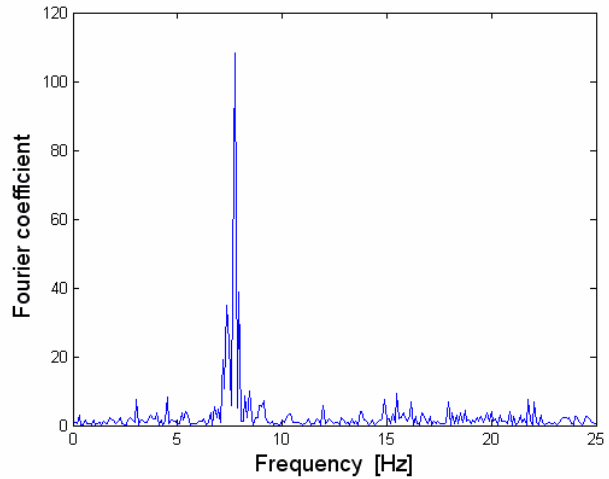


Fig. 29 FFT-spectrum of the relative velocity direction

The results for the spectra of these time series (figure 28, figure 29) show two distinct peaks for the velocity magnitude and only one peak for the direction. To analyse the complete flow field, the FFT was used in every point of the vector field and the results of the single FFT analyses was summed up and normalised by the maximum. For the summation only points of the flow field were used with more then 450 valid velocity vectors, from the 510 possible. More than 98% of the points of the flow field verify this condition.

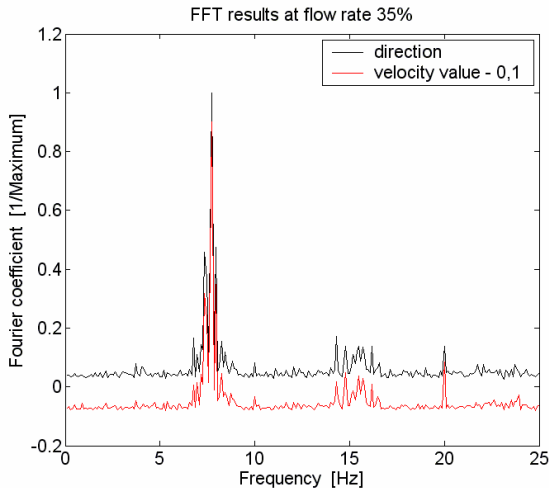


Fig. 30 Standardised summation of the amplitude spectra $Q/Q_0=0.35$

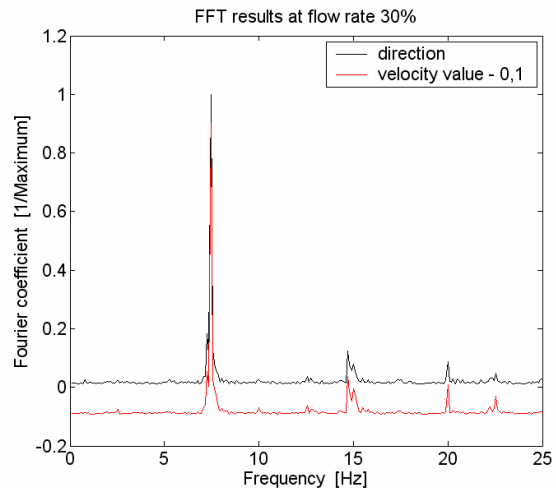


Fig. 31 Standardised summation of the amplitude spectra $Q/Q_0=0.30$

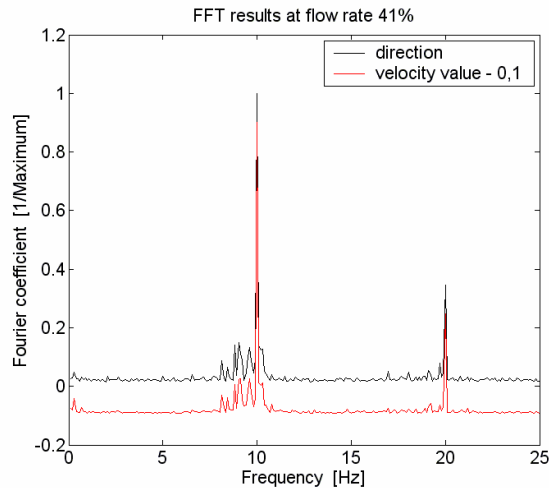


Fig. 32 Standardised summation of the amplitude spectra $Q/Q_0=0.41$

Figures 30 to 32 represent the results of these calculations. For a better visibility of the curves, a constant value of 0.1 has been subtracted from the spectrum for the velocity magnitude, thus these curves are delayed to the bottom of the graph. It can be seen from these figures that a very characteristic frequency appears for all tree flow rates examined here. Sometimes the second and third harmonics of this frequency are also visible. These results mean, that the whole flow field is changing with a characteristic frequency of e.g. 7.75 Hz at a flow rate of $Q/Q_0=0.35$.

This frequency corresponds to a time of 129 ms. With the time delay of 20 ms between two successive images it follows that 6 to 7 images are needed for this changing. This corresponds to a number of images between the repetition of the flow pattern observed in chapter 3.

The velocity measurements were taken in the absolute coordinate system, that means that in the results the angular velocity of the impeller w_{im} is included. The angular velocity of the rotating stall w_{RS} then follows from the following equations with w_{me} , the measured angular velocity (7.75 Hz). Interesting is also the number of revolutions of the impeller for one revolution of the stall cell in the impeller (N_{RRS}).

$$w_{me} = f_{FFT}; \quad w_{RS} = w_{im} - w_{me}; \quad N_{RRS} = \frac{w_{im}}{w_{RS}};$$

From this equations follows that for a FFT result of $f_{FFT}=7.75$ Hz ($Q/Q_0=0.35$) that the rotating stall needs 4.44 revolutions of the impeller to be in the same channel once more. For a flow rate of $Q/Q_0=0.30$ (figure 31) the frequency obtained by FFT is 7.45 Hz. Thus the rotating stall needs 3.92 revolutions of the impeller for one turn. For a flow rate of $Q/Q_0=0.41$ (figure 32) can not identify a difference between the stall cell frequency and the impeller frequency. It is already presented in Table 1 the stall cell moves in that case unsteady through the impeller.

5 SUMMARY

Time resolved PIV measurements have been used to determine the velocity fields in a rotating radial pump impeller. By the use of this PIV method it was possible to capture unsteady flow phenomena appearing in the impeller at throttled flow rate. A spacial stabilised stall cell has been observed, which starts to rotate inside the impeller (rotating stall) if the flow rate is decreased further. The FFT-analysis used to obtain the circumferential speed of the stall cell shows that the speed of the impeller and that of the stall cell differ more and more if the flow rate is reduced.

Further measurements will be performed, modifying the impeller parameters, to investigate their influence on the rotating stall, its circumferential speed and the initiation point. With higher temporal resolution the birth and death of a stall cell will be observed.

ACKNOWLEDGEMENTS

The authors thank the Dantec Dynamics GmbH for the support which made these experiments possible.

Corresponding author: Dr. -Ing. Elemér Pap, Postfach 4120, D-39016 Magdeburg, Germany
 Tel.: (+49) 391-6712427, Fax: (+49) 391-6712095
 Email: elemer.pap@vst.uni-magdeburg.de

REFERENCES

- Day I. J. (1993). "Stall inception in axial flow compressors". Transactions of ASME-Journal of Turbomachinery, 115, pp. 1 - 9
- Dobat A., Saathoff H., Wulff D. (2001). "Experimentelle Untersuchungen zur Entstehung von Rotating Stall in Axialventilatoren". Proc. Ventilatoren: Entwicklung - Planung - Betrieb, Braunschweig, Germany
- Emmons H. W., Pearson C. E., Grant H. P. (1955). "Compressor surge and stall propagation". Transaction of ASME, 79, pp. 455 - 469
- Escuret J. F., Garnier V. (1996). "Stall inception measurements in a high-speed multistage compressor". Transactions of ASME-Journal of Turbomachinery, 118, pp. 690 - 696
- Garnier V. H., Epstein A. H., Greitzer E. M. (1991). "Rotating waves as a stall inception indication in axial compressors". Transactions of ASME-Journal of Turbomachinery, 113, pp. 290 - 302
- Höss B., Leinhos D., Fottner L. (2000). "Stall inception in the compressor system of a turbofan engine". Transactions of ASME-Journal of Turbomachinery, 122, pp. 32 - 44
- Inoue M. (2000). "Propagation of multiple short-length-scale stall cells in an axial compressor rotor". Transactions of ASME-Journal of Turbomachinery, 122, pp. 45 - 54
- Katz M. (2002). "Aktive Unterdrückung von Rotating Stall in einem Axialverdichter mit pulsierender Lufteinblasung". Dissertation thesis. TU Darmstadt, Darmstadt, Germany
- Pap E., Lanzke A. (1999). "Untersuchung des Strömungsfeldes in einer Flüssigkeit-Gas-Strömung mittels Particle Image Velocimetry". Proc. 7. Fachtagung Lasermethoden in der Strömungsmeßtechnik, Saint - Louis, France
- Pap E., Lanzke A., Kalmar L. (2001). "Untersuchung des Einflusses auf das Strömungsfeld im radialen Pumpenlaufrad bei der Förderung von Gas-Flüssigkeitsgemisch", Budapest, Hungary
- Place J. M. M., Howard M. A., Cumpsty N. A. (1996). "Simulating the multistage environment for single-stage compressor experiments". Transactions of ASME-Journal of Turbomachinery, 118, pp. 706 - 716
- Saxer-Felici H. M., Saxer A. P., Inderbitzin A., Gyarmathy G. (1999). "Structure and propagation of rotating stall in a single- and a multi-stage axial compressor". Proc. International Gas Turbine and Aeroengine Congress and Exhibition, Indianapolis, Indiana, USA
- Sieverding C. H., Arts T., Denos R., Brouckaert J. F. (2000). "Measurement techniques for unsteady flows in turbomachines". Experiments in Fluids, 28, pp. 285-321
- Surek D. (2001). "Kombination von Radial- und Seitenkanalstufen für Turboverdichter". Forschung im Ingenieurwesen, 66, pp. 193-210
- TheMathWorks I. (2002). "Matlab user handbook".
- Ulbricht I. (2002). "Stabilität des stehenden Ringgitters". Dissertation thesis. TU Berlin, Berlin, Germany
- Wernet M. P. (2000). "Application of DPIV to study both steady state and transient turbomachinery flows". Optics & Laser Technology, 32, pp. 497-525